A Simulation Program for the Sensitivity and Linearity of Piezoresistive Pressure Sensors

Liwei Lin, *Member, IEEE,* Huey-Chi Chu, and Yen-Wen Lu

***Abstract*—A simulation program is developed which is capable of calculating the output responses of piezoresistive pressure sensors as a function of pressure and temperature. Analytical models based on small and large deflection theories have been applied to predict the sensitivity and linearity of pressure sensors. Surface-micromachined diaphragms with square or circular shapes, fabricated by a low pressure chemical vapor deposition sealing process, are designed and tested to verify the program. They are made of polysilicon and have a standard width (diameter) of 100 μm and thickness from 1.5 to 2.2 μm. Various parameters of the piezoresistive sensing resistors, including length, orientation, and dopant concentration, have been derived and constructed on top of the diaphragms. For a 100-μm-wide 2-μm-thick square-shape pressure sensor, calculated and experimental results show that sensitivity of 0.24 mV/V/(lbf/in^2) is achieved. Experimentally, a maximum linearity error of $\pm$0.1% full-scale span) is found on a 100-μm-wide 2.2-μm-thick square-shape pressure sensor. Both sensitivity and linearity are characterized by the diaphragm thickness and the length of the sensing resistors. [394]**

NOMENCLATURE

C_1, C_2, C_3	Constants to be determined in estimating radial displacement of circular plates.
D	Bending stiffness.
E	Young's modulus.
E_f	Fermi energy.
N	Dopant concentration.
R	Resistance.
T	Temperature.
V	Voltage.
V_1, V_2	Strain energy due to bending and stretching of middle planes, respectively.
Π	Piezoresistance coefficient.
a	Width of a square or rectangular plate or radius of a circular plate.
b	Length of a rectangular plate.
h	Plate thickness.
q	Applied pressure.
q_1, q_2	Applied pressure due to bending and membrane stresses, respectively.
r	Polar coordinates.
u, v, w	Displacement.
w_0	Maximum deflection.
ϵ	Strain.
ν	Poisson's ratio.

Subscripts

eff	Effective.
int	Input.
non	Noneffective.
out	Output.
x, y, z	Cartesian coordinates.
r	Radial.
θ	Circumferential.

Manuscript received October 15, 1998; revised August 3, 1999. This work was supported in part by the National Science Foundation under NSF CAREER Award ECS-9734421 and by NSF GOALI Award CMS-9800482. Subject Editor, G. Stemme.

L. Lin was with the Department of Mechanical Engineering and Applied Mechanics, University of Michigan, Ann Arbor, MI 48109–2125 USA. He is now with the Mechanical Engineering Department, University of California at Berkeley, Berkeley, CA 94720-1740 USA (lwlin@me.berkeley.edu).

H.-C. Chu is with the Institute of Applied Mechanics, National Taiwan University, Taipei, Taiwan, R.O.C.

Y.-W. Lu is with the Mechanical and Aerospace Department, University of California at Los Angeles, Los Angeles, CA 90024 USA.

Publisher Item Identifier S 1057-7157(99)09601-8.

I. INTRODUCTION

IN RECENT years, substantial research has been carried out on micromachined, diaphragm-type pressure sensors [1]–[5]. These sensors are fabricated by means of new manufacturing technologies such as bulk-micromachining [6], [7] or surface-micromachining [8], [9]. Many of them use silicon and its piezoresistivity as the detection mechanism. These transducers function when the resistivity of the sensing resistor changes as the diaphragm deflects due to applied pressure. In order to increase the sensitivity, the diaphragm thickness should be thin to maximize the load-deflection responses. On the other hand, thin diaphragm under high pressure may result in large deflection and nonlinear effects that are not desirable. It is therefore important to characterize the relationship between diaphragm thickness, deflection, and linearity, both analytically and experimentally in order to establish the design guidelines for micropressure sensors.

Numerical simulations such as finite element methods can be used to simulate load-deflection relationships, including nonlinear effects of thin diaphragms. However, analytical solutions are preferred in the design stage to provide prompt and reliable predictions. Previously, analytical investigations on the diaphragm deflections have been reported, including the theoretical studies on square- and circular-shape diaphragms [10], new analytical solutions for square-shape diaphragms [11], and the applications of diaphragm deflections to the characterizations of thin film mechanical properties [12]. Moreover, different types of diaphragms and processes have been designed to increase the sensitivity and improve the linear-

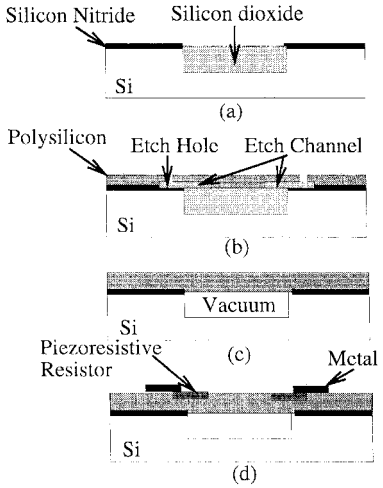

Fig. 1. Process flow of a surface-micromachined pressure sensor.

ity. For example, microdiaphragms have been constructed with stress concentration structures to increase the sensitivity [13]–[15]. As the field of microelectromechanical systems (MEMS) continues to expand, diaphragm-based structures may find abundant applications. Both sensitivity and linearity will be important issues to be investigated.

Several previous reports have found strange nonlinear effects, including convex and concave types of nonlinear characteristics with respect to different pressure inputs [16], [17]. In the case of capacitive pressure sensors, large deflection for square-shape diaphragms have been studied [18] by using Hooke's method [19]. In order to provide a complete analytical tool for sensitivity and linearity analyses, this paper uses surface-micromachined, piezoresistive pressure sensors as the drive to develop a simulation program. Absolute-type pressure sensors which use vacuum cavities as the reference pressure are fabricated by a low-pressure chemical vapor deposition (LPCVD) sealing process [20]. Theoretical derivations based on the mechanics of small and large deflections have been applied to study the sensitivity and to predict the nonlinear behavior. Finally, a simulation program has been developed and is available on the internet for free download [21] to simulate both the sensitivity and linearity responses of pressure sensors.

II. Pressure Sensor Topologies and Fabrication Processes

Both square- and circular-shape diaphragms have been designed, fabricated, and characterized. These pressure sensors are constructed with surface-micromachined diaphragms by a micromachining process which uses LPCVD sealing to create vacuum cavities [20]. The process starts with cleaning the wafer. A thin layer, 0.15 μm, of LPCVD silicon nitride is then deposited. The cavity area is defined by a first mask via dry etching process to etch into the silicon of 1 μm in depth. The wafer then goes through a thermal oxidation process to create about 2-μm-thick silicon dioxide at the cavity area and to construct a flat surface, as illustrated in Fig. 1(a). LPCVD oxide of 0.5 μm is then deposited to form the etch channels. These etch channels are defined by dry etching with a second mask. It is

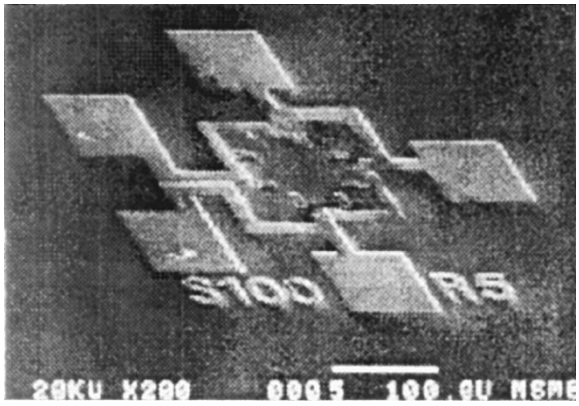

Fig. 2. SEM microphoto of a fabricated micropressure sensor with 100-μm-wide square-shape diaphragm.

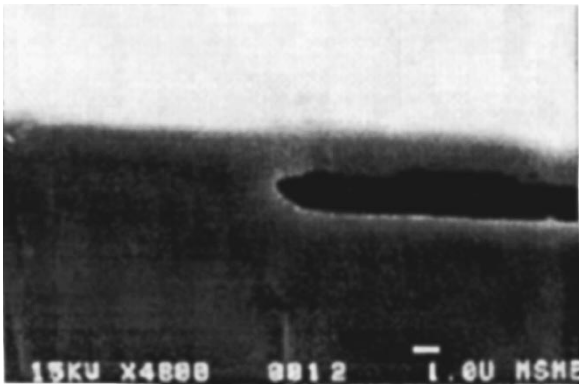

Fig. 3. SEM microphoto showing the cross-sectional view of a cleaved cavity. The depth of the cavity is about 2 μm.

followed by a 1-μm LPCVD polysilicon deposition, etch holes patterning (mask 3), and dry etching, as shown in Fig. 1(b). The oxide in the etch channels and the cavity are now cleared by concentrated hydrofluoric acid (HF) etching. The second layer of polysilicon with 1 μm in thickness is then deposited by a second LPCVD polysilicon deposition step, which seals the etch holes and channels and creates a vacuum environment inside the cavity [22]. The cross-sectional view at the end of this step is shown in Fig. 1(c). The piezoresistive resistors are then constructed by using a fourth mask on top the diaphragm made of undoped-polysilicon. Boron is implanted at an energy of 25 keV and a dose of 10^{15} cm^{-2}. An LPCVD oxide passivation layer is deposited with contact holes opened by using the fifth mask. Aluminum deposition and patterning (mask 6) are then followed to finish the process, as shown in Fig. 1(d).

Fig. 2 is a scanning electron microscope (SEM) micrograph of a fabricated pressure sensor. The size of the square diaphragm is 100 μm in width. There are eight etch channels around the diaphragm as access channels to remove the sacrificial oxide inside the cavity. Aluminum metal pads can be clearly identified in this figure. Circular-shape diaphragms have also been fabricated with various sizes. Fig. 3 shows the SEM micrograph of a cleaved pressure sensor. This cross-sectional view shows both the cavity and the thin diaphragm. In this case, the depth of the cavity is 2 μm and the thickness of the diaphragm is 2 μm.

III. Sensitivity Analyses

The sensitivity analyses are based on small deflection theories of plates. In classic mechanics, analytical solutions can be found for the pressure-deflection relationships of plates made of isotropic, homogeneous, linearly elastic materials [10]. Analytical models have been established for diaphragms with simple geometry such as square, rectangular, and circular shapes. For the case of circular-shape diaphragms under small deflection, the radial and circumferential strain with respect to the applied pressure can be derived as [10]

$$\epsilon_r = \frac{-3qa^2(1-\nu^2)}{8Eh^2}\left(1-\frac{3r^2}{a^2}\right) \tag{1}$$

$$\epsilon_\theta = \frac{-3qa^2(1-\nu^2)}{8Eh^2}\left(1-\frac{r^2}{a^2}\right) \tag{2}$$

where q is the applied pressure, E is the Young's modulus, and ν is Poisson's ratio. The thickness of the diaphragm is represented as h and the radius as a. Subscripts r and θ represent the radial and circumferential directions, respectively.

For the case of square-shape diaphragm under small deflection, a combination method suggested by Timoshenko is used in this paper [10]. It is assumed that the total deflection of a rectangular-shape plate with clamped edges is the summation of three components: w_1, w_2, and w_3. The first component, w_1, comes from the deflection of a simply supported plate under the same applied pressure. The second and third components are introduced to preserve the clamped boundary conditions. The following equations are derived for a rectangular plate with widths of a and b and bending stiffness D under an applied pressure q.

$$w_1 = \frac{4qa^4}{\pi^5 D}\sum_{m=\text{odd}}^{\infty}\frac{(-1)^{\frac{m-1}{2}}}{m^5}\cos\frac{m\pi x}{a} \cdot\left(1-\frac{(A_m\tanh A_m+2)\cosh\frac{m\pi y}{a}}{2\cosh A_m}+\frac{\frac{m\pi y}{a}\sinh\frac{m\pi y}{a}}{2\cosh A_m}\right) \tag{3}$$

$$w_2 = \frac{-a^2}{2\pi^2 D}\sum_{m=\text{odd}}^{\infty}\frac{E_m(-1)^{\frac{m-1}{2}}\cos\frac{m\pi x}{a}}{m^2\cosh A_m} \cdot\left(\frac{m\pi y}{a}\sinh\frac{m\pi y}{a}-A_m\tanh A_m\cosh\frac{m\pi y}{a}\right) \tag{4}$$

$$w_3 = \frac{-b^2}{2\pi^2 D}\sum_{m=\text{odd}}^{\infty}\frac{F_m(-1)^{\frac{m-1}{2}}\cos\frac{m\pi y}{b}}{m^2\cosh B_m} \cdot\left(\frac{m\pi x}{b}\sinh\frac{m\pi x}{b}-B_m\tanh B_m\cosh\frac{m\pi x}{b}\right) \tag{5}$$

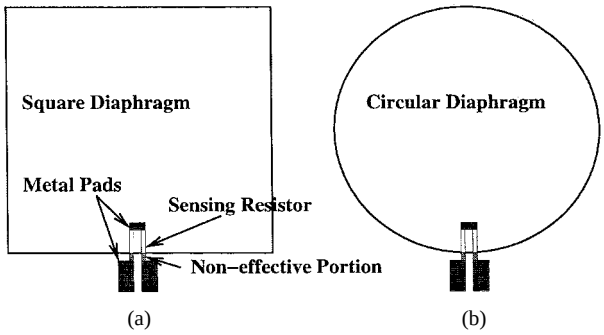

Fig. 4. Most sensitive positions for square and circular diaphragms.

where

$$A_m = \frac{m\pi b}{2a} \tag{6}$$

$$B_m = \frac{m\pi a}{2b}. \tag{7}$$

Both E_m and F_m are solved by (8) and (9), shown at the bottom of the page, and

$$w = w_1 + w_2 + w_3. \tag{10}$$

The strain is solved by

$$\epsilon_{xx} = -z\frac{\partial^2 w}{\partial x^2} \tag{11}$$

$$\epsilon_{yy} = -z\frac{\partial^2 w}{\partial y^2} \tag{12}$$

$$\epsilon_{xy} = -2z\frac{\partial^2 w}{\partial x\partial y}. \tag{13}$$

These analytical derivations determine the most sensitive places and orientations for piezoresistive resistors [23]. For square-shape membranes, resistors should be placed at the middle and close to the edge with a direction perpendicular to the edge, as shown in Fig. 4(a). For circular-shape diaphragm, the most sensitive place is at the edge with resistors placed in the radial directions, as shown in Fig. 4(b). Moreover, these resistors should be deposited either close to the top or bottom of the diaphragms for maximum sensitivity. These placement are well known in the sensor community that validates the correctness of the above analytical models.

Once the strain distribution on a diaphragm under an applied pressure is calculated, various characteristics of the sensing resistor, including sheet resistance, width, and geometry, can be analyzed. The sensing resistors are connected as a half

$$\frac{4qa^2A_n}{\pi^3n^4\cosh^2 A_n}-\tanh A_n = \frac{E_n}{n}\left(\tanh A_n+\frac{A_n}{\cosh^2 A_n}\right)+\frac{8na}{\pi b}\sum_{m=\text{odd}}^{\infty}F_m\frac{1}{m^3\left(\frac{a^2}{b^2}+\frac{n^2}{m^2}\right)^2} \tag{8}$$

$$\frac{4qb^2B_n}{\pi^3n^4\cosh^2 B_n}-\tanh B_n = \frac{F_n}{n}\left(\tanh B_n+\frac{B_n}{\cosh^2 B_n}\right)+\frac{8nb}{\pi a}\sum_{m=\text{odd}}^{\infty}E_m\frac{1}{m^3\left(\frac{a^2}{b^2}+\frac{n^2}{m^2}\right)^2} \tag{9}$$

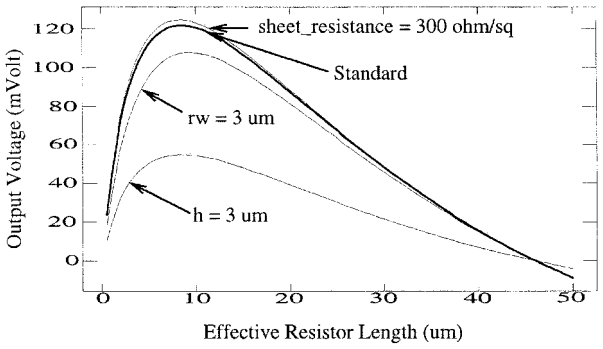

Fig. 5. Sensitivity analysis of a square-shape diaphragm.

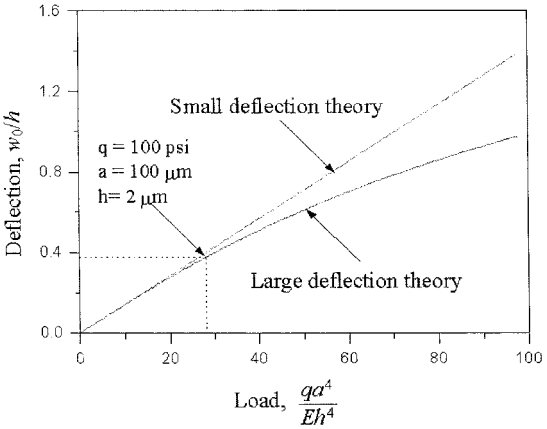

Fig. 6. Dimensionless deflection-load diagram for clamped circular plates.

Wheatstone bridge with two sensing resistors placed inside the diaphragm, and the other two reference resistors located outside the diaphragm. The output voltage is calculated as

$$V_{\text{out}} = \frac{\Delta R_{\text{eff}}}{2(R_{\text{eff}} + R_{\text{non}}) + \Delta R_{\text{eff}}} V_{\text{in}} \tag{14}$$

where R_{eff} is the effective resistance from the sensing resistor. R_{non} is the noneffective resistance from the noneffective portion of the resistor, as well as the contributions from components such as metal pads and contact resistance. When an input voltage of 5 V and a pressure of 100 lbf/in^2 is applied, Fig. 5 shows the sensitivity simulations with respect to the effective length of the resistors for a square-shape diaphragm with a width of 100 μm. Gauge factors of 36.1 and -7.4 for parallel and perpendicular directions are used in the simulation based on the best fit from experimental outputs. The standard-type resistor has a sheet resistance of 200 Ω/square, a width of 2 μm, and noneffective length of 2 μm. It is found that when the resistor length is about 10 μm (effective length of 8 μm), a maximum output voltage around 120 mV is achieved. Several parameters are simulated to examine the sensitivity responses. For example, increasing the sheet resistance to 300 Ω/square can slightly increase the sensitivity. On the other hand, increasing the width of the resistor from 2 to 3 μm will drop the output level about 15%. These phenomena can be explained by examining (14) where R_{non} at the denominator has components that are independent of the sheet resistance. Therefore, if the resistance of the sensing resistor is increased (by increasing the sheet resistance) or decreased (by increasing the width), the output voltage increases or decreases, accordingly. Finally, increasing the diaphragm thickness will drastically reduce the sensor output as the sensitivity drops.

The circular-shape diaphragms are found to have similar characteristics as the square ones. In order to simulate diaphragms with different kinds of geometry and property, a simulation program has been developed for both the square and circular diaphragms [21]. Researchers interested in the optimal designs of different diaphragm sizes and sensing resistors can download this program to conduct their own simulations. Typical inputs for this program are the shape of the diaphragm (rectangular or circular), dimensions of the diaphragm (width, diameter, thickness), pressure range, placement of the resistors, and properties of the resistors.

IV. Linearity Characterization

The linearity analysis begins with small deflection theories where the deflections are small compared with the thickness of the diaphragm. Fig. 6 shows the simulation result of dimensionless deflection with respect to dimensionless load by using small and large deflection theories, respectively. For a circular diaphragm with diameter of 100 μm, thickness of 2 μm, and under a pressure of 100 lbf/in^2, the load-deflection relation actually enters large deflection regime as indicated in Fig. 6. When large deflection effects are considered, the strain-displacement relations are no longer linear and they are expressed as

$$\epsilon_{xx} = \frac{\partial u}{\partial x} + \frac{1}{2}\left(\frac{\partial w}{\partial x}\right)^2 \tag{15}$$

$$\epsilon_{yy} = \frac{\partial v}{\partial y} + \frac{1}{2}\left(\frac{\partial w}{\partial y}\right)^2 \tag{16}$$

$$\epsilon_{xy} = \frac{1}{2}\left(\frac{\partial u}{\partial y} + \frac{\partial v}{\partial x}\right) + \left(\frac{\partial w}{\partial x}\frac{\partial w}{\partial y}\right). \tag{17}$$

The large deflection problem can be solved under different boundary conditions. However, only a few cases can be solved analytically, and many of the problems have to be solved numerically. In the case of simple geometry, both square- and circular-shape diaphragms can be solved analytically.

A. Large Deflection of Clamped Circular Plates

In order to solve the large deflection problem for clamped circular plates, strain energy method is used [24]. For a deflected circular plate, the stored strain energy is first separated into two parts, the energy of bending V_1 and the energy due to the stretching of the middle plane V_2. The strain energy due to bending is derived by beginning with the small deflection assumptions

$$w = w_0\left(1 - \frac{r^2}{a^2}\right)^2 \tag{18}$$

and V_1 is expressed as

$$V_1 = \frac{32\pi w_0^2 D}{3a^2}. \tag{19}$$

The energy due to the stretching of the middle plane is derived by assuming that the radial displacement u matches the clamped boundary conditions as well as the center position of the plate

$$u = r(a-r)(C_1 + C_2 r + C_3 r^2 + \cdots). \tag{20}$$

If the first two terms in (20) are considered, constants C_1 and C_2 can be determined by taking the total energy of the plate for an equilibrium position in a minimum. Therefore, both constants can be determined

$$C_1 = 1.185\frac{w_0^2}{a^3} \tag{21}$$

$$C_2 = -1.75\frac{w_0^2}{a^4} \tag{22}$$

and V_2 can be derived as

$$V_2 = 2.59\pi D\frac{w_0^4}{a^2h^2}. \tag{23}$$

The total strain energy is the combination of V_1 and V_2. Based on the principle of virtual displacement

$$\frac{d(V_1+V_2)}{dw_0}\delta w_0 = 2\pi q\delta w_0\int_0^a\left(1-\frac{r^2}{a^2}\right)^2 r\,dr. \tag{24}$$

The maximum deflection is derived as

$$w_0 = \frac{qa^4}{64D}\frac{1}{\left(1+0.488\frac{w_0^2}{h^2}\right)}. \tag{25}$$

Therefore, (25) can be used to calculate the maximum deflection if the loading is given. The deflection w can then be derived by using (18). The displacement u can be calculated by (20), and the stress and strain at any point of the diaphragm can be solved by using (15)–(17).

B. Large Deflection of Clamped Square Plates

The large deflection of square plates with clamped edges has been solved by different methods [25], [24], [26]. A combination method developed by Föppl is applied here [27]. This method combines the known solutions of small deflection theories on clamped boundary conditions and the membrane theories for large deflection problems on simply supported boundary conditions. First, the total loading q is divided into two parts, q_1 and q_2. The loading that is balanced by both the bending stresses and shearing stresses is represented by q_1. The loading that is balanced by the membrane stresses is represented by q_2. These two are calculated separately and combined together at the end.

The loading q_1 is derived from the small deflection theory as

$$q_1 = 71.3\frac{w_0Eh^3}{a^4}. \tag{26}$$

If the plate is considered a membrane, the maximum deflection can be derived [10], and the loading q_2 is represented as

$$q_2 = 31.1\frac{w_0^3Eh}{a^4}. \tag{27}$$

The total loading is the combination

$$q = \frac{w_0Eh^3}{a^4}\left(71.3+31.1\frac{w_0^3}{h^2}\right). \tag{28}$$

If the total loading is given, w_0 can be solved by the above equation, and q_1, q_2 can be derived, respectively. The stress and strain caused by q_1 at any given point of the square-shape diaphragm are calculated by using the classic small deflection theory of plates. The stress and strain caused by q_2 are calculated by the membrane theory. The total stress and strain at any given point are the sum of the two cases.

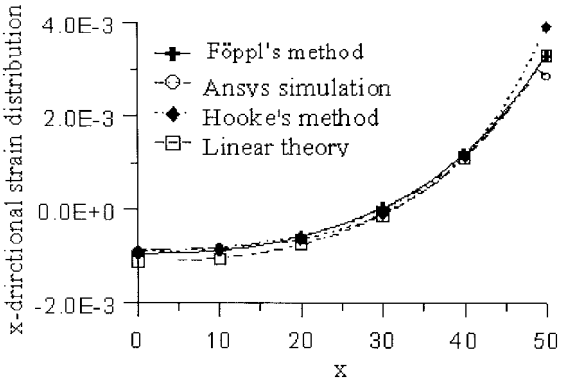

Fig. 7. Calculated x-directional strain distributions by linear theory, Föppl's method, Hook's method, and ANSYS simulation for a square diaphragm, 100 μm in width, 2 μm in thickness, and under a pressure of 100 lbf/in^2.

In order to verify the accuracy of the above derivations in the case of micromachined diaphragms, four different simulations have been conducted as shown in Fig. 7, including small deflection (linear) theory, Hooke's method [19], finite element method (ANSYS [28]), and Föppl's method. This figures shows the x-directional strain distributions for a square diaphragm of 100 μm in width, 2 μm in thickness, and under a pressure of 100 lbf/in^2. The Föppl's method agrees with ANSYS nonlinear simulation results well. The Hooke's approach deviates from other methods at regions close to the edges of the diaphragm where the piezoresistive sensors are placed. Therefore, Föppl's method appears to be a good choice for the analytical model.

V. Experimental Results and Discussions

A. Sensitivity and Linearity

Several micromachined pressure sensors were designed and fabricated based on the analytical model. The experimental and simulation results are based on the connection of a half Wheatstone bridge as described in the previous section. Under small deflection, the sensor is expected to behave linearly with respect to applied pressure. However, due to the existence of R_{non} as shown in (14), the nonlinear effect occurs

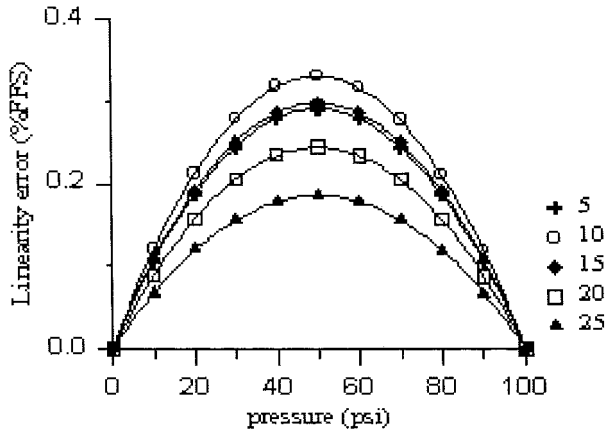

Fig. 8. Simulation result of linearity error with respect to input pressure by using the small deflection theory.

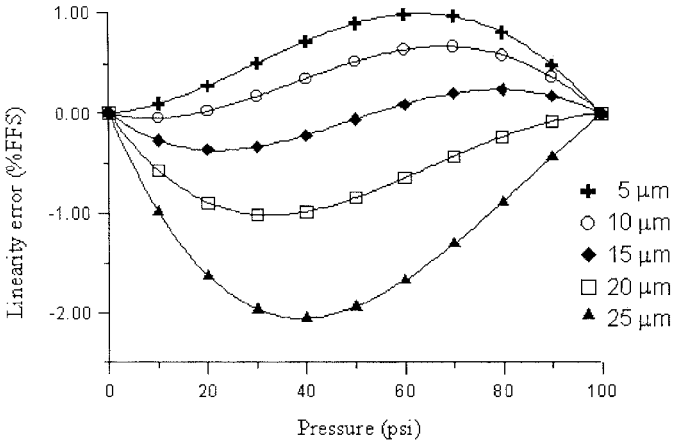

Fig. 9. Linearity error for a 100-μm-wide square diaphragm with a thickness of 2 μm and various resistor lengths.

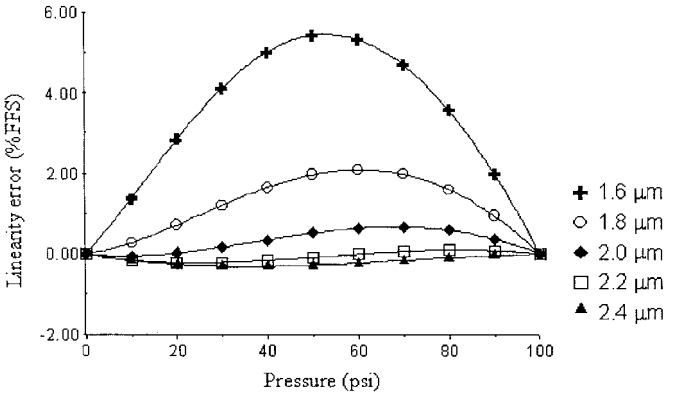

Fig. 10. Linearity error for a 100-μm-wide square diaphragm with a resistor length of 10 μm and various diaphragm thickness.

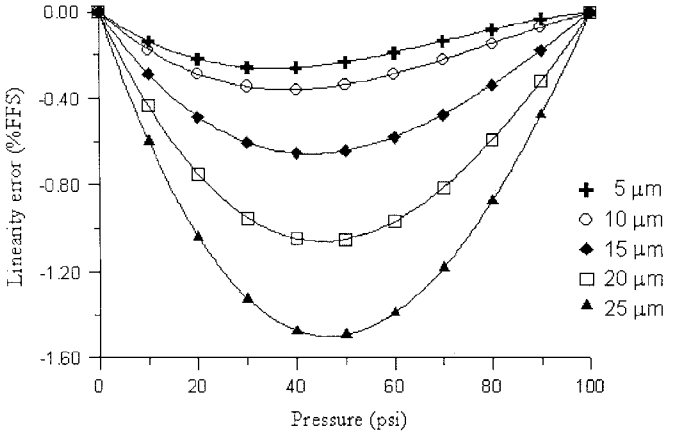

Fig. 11. Linearity error for 100 μm in diameter, circular diaphragm with 2 μm in thickness, and various resistor lengths.

even though all the other components change linearly under small deflection. Fig. 8 is the linearity simulation of square diaphragms under small deflection (linear theory). The sensors have widths of 100 μm (square shape) and thickness of 2 μm, and the resistors have lengths from 5 to 25 μm. The linearity error is less than 0.3% full-scale span (FSS). Moreover, nonlinear effects differ when the length of the resistor changes. The 10-μm-long resistor has the best sensitivity from the result of sensitivity simulation, but has the worst linearity error of about 0.3% as shown. The linearity error seems to decrease as the length of the resistor increases. Moreover, the linearity curves are symmetrical to the central pressure at 50 lbf/in^2.

When large deflection effects are considered, the shape of the curves changes. Fig. 9 shows the simulation result by using the large deflection effects as discussed. First, the absolute magnitude error is much larger than the linearity error derived from small deflection theories. Second, the shape of the curve differs as the length of the sensing resistor changes. Third, the error may go from negative to positive as the applied pressure changes. Finally, the shape of the linearity error is no longer symmetrical to the central pressure and becomes irregular. According to the simulation results in Fig. 9, minimum average error is achieved when the sensing resistor length is 15 μm. If the resistor length is fixed at 10 μm and the thickness of the diaphragm is changed, Fig. 10 shows the new simulation results. It is observed that when the diaphragm thickness increases from 1.6 to 2.4 μm, the linearity error reduces and changes signs from positive to negative, and the absolute value decreases as well. The best (minimum) average linearity error occurs when the diaphragm thickness is about 2.2 μm. It is noted that as the diaphragm thickness increases, the linearity error decreases and saturates.

A similar trend is found for diaphragms with circular shapes. Figs. 11 and 12 are simulation results for 100 μm in diameter circular-shape diaphragms. In Fig. 11, the thickness of the diaphragm is fixed at 2 μm, and in Fig. 12, the length of the sensing resistor is fixed at 10 μm. When the linearity error of square and circular diaphragms are compared at the same thickness, the circular ones have smaller linearity errors (see Figs. 10 and 12). This is probably due to the fact that the circular-shape diaphragms occupy less area than the square ones for the same diameter and width. The circular diaphragms are more rigid in this case, and large deflection effects are minimized.

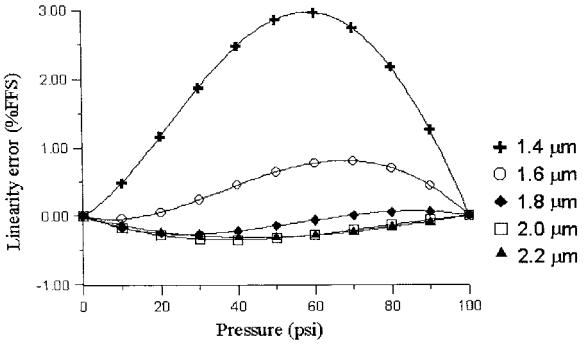

Fig. 12. Linearity error for 100 μm in diameter, circular diaphragm with resistor length of 10 μm, and various diaphragm thickness.

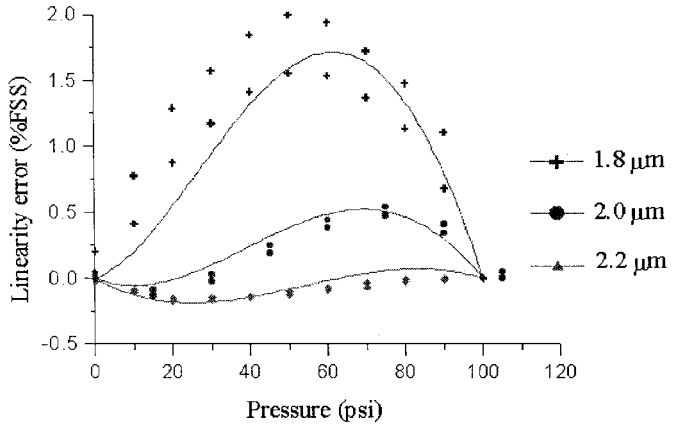

Fig. 13. Measured (symbols) and simulated (solid lines) linearity error of square-shape pressure sensors with different diaphragm thickness.

B. Experimental Results

The electrical responses of fabricated microsensors are collected by using a computer-controlled pressure supplier. Our experiments show that a sensitivity of 0.24 mV/V/(lbf/in^2) can be achieved. Moreover, the sensitivity increases as the thickness of the diaphragm decreases. The linearity error of a set of square-shape diaphragm pressure sensors with sensing resistor length of 10 μm is plotted in Fig. 13 by a measure of FSS with respect to the applied pressure. The symbols are the experimental measurements and the solid lines are the results from the simulation program. The best linearity error is about $\pm$0.1% FSS with pressure hysteresis of 0.02% FSS when the thickness of the diaphragm is 2.2 μm. It is observed that the measured data are consistent with the analytical predictions as shown in Fig. 10. The thinnest diaphragm not only has the highest linearity error but also has the largest hysteresis. From the experimental data and the theoretical simulations, it can be concluded that large deflection effect did occur and cause nonlinear responses.

C. Temperature Effects

Temperature affects the performance of the pressure sensors in several categories, including changes of geometry, material properties, and piezoresistivity. Both geometrical and material property changes only contribute less than 100 ppm, which is much smaller than the experimental result [29]. The change of piezoresistivity appears to dominate the temperature responses and is discussed in this section. The piezoresistance coefficients in silicon have been studied in a graphical representation [30]. It is found that the piezoresistance coefficient Π is a function of temperature T and dopant concentration N.

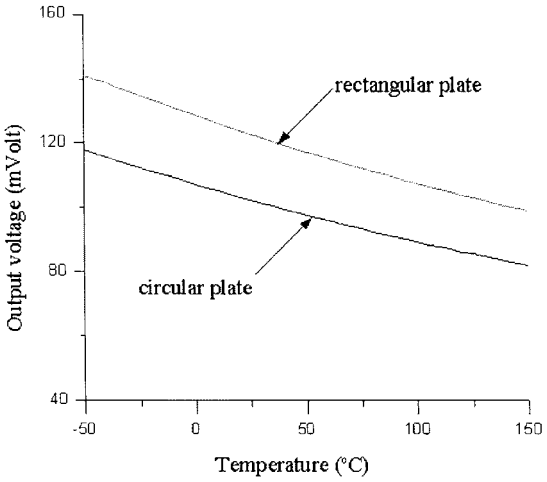

Fig. 14. Simulation result of temperature effects on square- and circular-shape (100 μm wide and 2 μm thick) pressure sensors.

$$\Pi(N,T) = \frac{300}{T\ln(1+e^{E_f/kT})(1+e^{-E_f/kT})}\Pi(300) \quad (29)$$

where $\Pi(N,T)$ is presented as a function of Fermi energy E_f, temperature T, and the piezoresistivity at 300 K, $\Pi(300)$. It is noted that this expression is only good for silicon, and more detailed studies on the temperature and piezoresistivity of polysilicon have been reported [31]–[33]. However, we found this expression is suitable for the first-order approximation in our case and was able to built this model into our simulation program. Fig. 14 shows the simulation results of maximum output voltage on both circular- and square-shape micropressure sensors with respect to temperature. These diaphragms have the characteristic length (width or diameter) of 100 μm, a thickness of 2 μm, and under an applied pressure of 100 lbf/in^2. The sensing resistors have the standard parameters of 2 μm in width. An offset of about 20 mV is observed because under the same characteristic length (100 μm), circular-shape diaphragms have stronger rigidity such that they are less sensitive than those square-shape diaphragms. It clearly indicates that when temperatures rise from room temperature to 100 °C, the sensitivity of both sensors may be reduced by about 15%. Moreover, at the same temperature and characteristic length, square-shape diaphragms are more sensitive than circular ones. Experimentally, tests have been conducted at three testing temperatures from $-$40 °C, 25 °C, to 120 °C, as shown by the symbols in Fig. 15. These data were collected from a 100-μm-wide 2-μm-thick square-shape micropressure sensor. It is found that our simulation model (solid lines) is consistent with the experimental result.

VI. Conclusion

In conclusion, this paper has demonstrated the feasibility of applying analytical models to the sensitivity and linearity

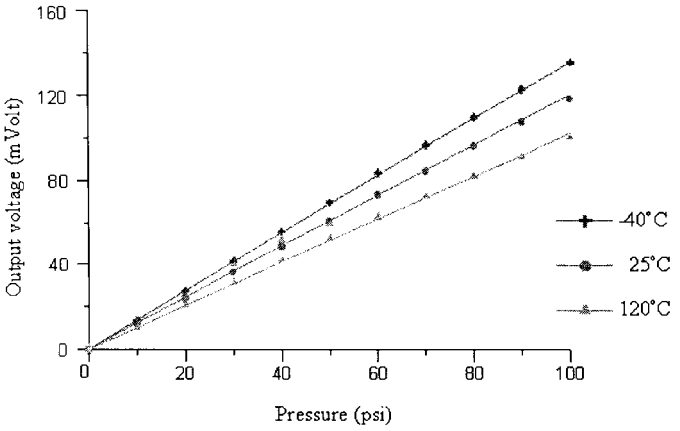

Fig. 15. Experimental (symbols) and simulation (lines) results of a square-shape (100 μm wide and 2 μm thick) pressure sensor under different temperature and pressure.

analyzes for surface-micromachined pressure sensors. A newly developed fabrication process has been used to fabricate these sensors which use the LPCVD process as the sealing mechanism. The sensitivity of the pressure sensors has been studied, and the design optimization processes have been established for both square- and circular-shape diaphragms. The problems of linearity have been investigated by using Föppl's method for square-shape diaphragms and the energy method for circular-shape diaphragms. It is found that both the length of the sensing resistors and the thickness of the diaphragm will affect the characteristics of linearity error. These results have been successfully verified on the prototype pressure sensors made by surface-micromachined diaphragms. Experimental results show that sensitivity of 0.24 mV/V/(lbf/in^2) on a 2.0-μm-thick square diaphragm is achieved. Furthermore, a linearity error of $\pm$0.1% FSS with pressure hysteresis of 0.02% FSS on a 2.2-μm-thick square diaphragm is accomplished. In order to disseminate these research results, a simulation program has been developed and placed on the internet for free download. It should be noted that these analytical models are capable of predicting sensor responses in various positions or directions on thin diaphragms. With simple modifications, the full Wheatstone bridge can be implemented into the program, and research is encouraged to exercise different pressure sensor designs.

ACKNOWLEDGMENT

The authors would like to thank Dr. W. Yun and Mr. T. Haniff at the SiTek Inc. for assisting in fabrication and data collections of the micropressure sensors.

REFERENCES

[1] W. H. Ko, "Solid-state capacitive pressure transducers," *Sens. Actuators*, vol. 10, pp. 303–320, 1986.
[2] H. L. Chau and K. D. Wise, "Scaling limits in batch-fabricated silicon pressure sensors," *IEEE Trans. Electron Devices*, vol. ED-34, pp. 850–858, 1987.
[3] K. Suzuki, S. Suwazono, and T. Ishihara, "$C_{\rm mos}$ integrated silicon pressure sensor," *IEEE J. Solid-State Circuits*, vol. SSC-22, pp. 151–156, 1987.
[4] J. T. Kung and H.-S. Lee, "An integrated air-gap-capacitor pressure sensor and digital readout with sub-100 attofarad resolution," *IEEE J. Microelectromech. Syst.*, vol. 1, pp. 121–129, 1992.
[5] C. H. Mastrangelo, X. Zhang, and W. C. Tang, "Surface-micromachined capacitive differential pressure sensor with lithographically defined silicon diaphragm," *IEEE J. Microelectromech. Syst.*, vol. 5, pp. 89–105, 1996.
[6] S. K. Clark and K. D. Wise, "Pressure sensitivity in anisotropically etched thin-diaphragm pressure sensors," *IEEE Trans. Electron Devices*, vol. ED-26, pp. 1887–1896, 1979.
[7] Motorola Semiconductor Products Sector, *Pressure Sensors—Device Data*, Phoenix, AZ, 1994.
[8] H. Guckel, "Surface micromachined pressure transducers," *Sens. Actuators*, vol. A28, pp. 133–146, 1991.
[9] S. Sugiyama, K. Shimaoka, and O. Tabata, "Surface micromachined micro-diaphragm pressure sensors," in *Proc. 6th Int. Conf. Solid-State Sensors and Actuators (Transducers'91)*, 1991, pp. 188–191.
[10] S. P. Timoshenko and S. Woinowsky-Krieger, *Theory of Plates and Shells*, 2nd ed. New York: McGraw-Hill, 1970.
[11] D. Maier-Schneider, J. Maibach, and E. Obermeier, "A new analytical solution for the load-deflection of square membranes," *IEEE J. Microelectromech. Syst.*, vol. 4, pp. 238–241, 1995.
[12] M. G. Allen, M. Mehregany, R. T. Howe, and S. D. Senturia, "Microfabricated structures for the *insitu* measurement of residual stress, young's modulus, and ultimate strain of thin films," *Appl. Phys. Lett.*, vol. 51, pp. 241–243, 1987.
[13] M. Bao, L. Yu, and Y. Wang, "Stress concentration structure with front beam for pressure sensor," *Sens. Actuators*, vol. A28, pp. 105–112, 1991.
[14] H. Sandmaier and K. Kuhl, "A square-diaphragm piezoresistive pressure sensor with a rectangular central boss for low-pressure ranges," *IEEE Trans. Electron Devices*, vol. 40, pp. 1754–1759, 1993.
[15] S. Hein, V. Schlichting, and E. Obermeier, "Piezoresistive silicon sensor for very low pressures based on the concept of stress concentration," in *Proc. 7th Int. Conf. Solid-State Sensors and Actuators (Transducers'93)*, 1993, pp. 628–631.
[16] K. Yamada, M. Nishihara, and R. Kanzawa, "A piezoresistive integrated pressure sensor," *Sens. Actuators*, vol. 4, pp. 63–69, 1983.
[17] Y. Matsuoka *et al.*, "Characteristic analysis of a pressure sensor using the silicon piezoresistance effect for high-pressure measurements," *J. Micromech. Microeng.*, vol. 5, pp. 25–31, 1995.
[18] L. Tong, J.-T. Hsu, W. Ko, and X. Ding, "The analysis of capacitive pressure sensor with large deflection," in *Proc. 6th Int. Conf. Solid-State Sensors and Actuators (Transducers'93)*, 1993, pp. 185–187.
[19] R. Hooke, "Approximate analysis of the large deflection elastic behavior of clamped, uniformly loaded, rectangular plates," *J. Mech. Eng. Sci.*, vol. 11, pp. 256–268, 1969.
[20] W. Yun, L. Lin, and T. Haniff, "Method of making a surface micromachined silicon pressure sensors," U.S. Patent 5,759,870, 1998.
[21] L. Lin. (1998), *Simulation Program for Piezoresistive Pressure Sensors*. [Online]. Available HTTP: http://www.me.berkeley.edu/∼lwlin
[22] L. Lin, K. M. McNair, R. T. Howe, and A. P. Pisano, "Vacuum encapsulated lateral microresonators," in *Dig. Int. Conf. Solid-State Sensors and Actuators (Transducers'93)*, 1993, pp. 270–273.
[23] L. Lin and W. Yun, "Design, optimization and fabrication of surface micromachined pressure sensors," to be published.
[24] R. Szilard, *Theory and Analysis of Plates: Classical and Numerical Methods*. Englewood Cliffs, NJ: Prentice-Hall, 1974.
[25] H. M. Berger, *J. Appl. Mechanics*, vol. 22, p. 465, 1955.
[26] C.-Y. Chia, *Nonlinear Analysis of Plates*. New York: McGraw-Hill, 1980.
[27] A. Föppl, *Drang und Zwang*, vol. 1, p. 345, 1924.
[28] ANSYS, *Finite Element Analysis Program*, Swanson Analysis Systems, Inc., ANSYS Inc., Canonsbury, PA, 1996.
[29] H.-C. Chu, "Surface micromachined piezoresistive pressure sensors," M.S. thesis, Nat. Taiwan Univ., Inst. of Appl. Mechanics, Taipei, Taiwan, 1996.
[30] Y. Kanda, "A graphical representation of the piezoresistance coefficients in silicon," *IEEE Trans. Electron Devices*, vol. ED-29, pp. 64–70, 1982.
[31] V. Mosser, J. Suski, J. Goss, and E. Obermeier, "Piezoresistive pressure sensors based on polycrystalline silicon," *Sens. Actuators*, vol. A28, pp. 113–131, 1991.
[32] E. Obermeier and P. Kopystynski, "Polysilicon as a material for microsensor applications," *Sens. Actuators*, vol. A30, pp. 149–155, 1992.
[33] G. Shuwen, T. Songshen, and W. Wang, "Temperature characteristics of microcrystalline and polycrystalline silicon pressure sensor," *Sens. Actuators*, vol. A21–23, pp. 133–136, 1990.

Liwei Lin (S'92–M'93) received the B.S. degree in power mechanical engineering from National Tsing Hua University, Taiwan, R.O.C., in 1986, the M.S. and Ph.D. degrees in mechanical engineering from the University of California, Berkeley, in 1991 and 1993 respectively.

He was with BEI Electronics Inc. USA from 1993 to 1994 in research and development of microsensors. From 1994 to 1996, he was an Associate Professor with the Institute of Applied Mechanics, National Taiwan University, Taiwan. From 1996 to 1999, he was an Assistant Professor with the Mechanical Engineering and Applied Mechanics Department, University of Michigan. Since 1999, he has been an Assistant Professor with the Mechanical Engineering Department and Associate Director at the Berkeley Sensor and Actuator Center, University of California at Berkeley. His research interests are in microelectromechanical systems, including design, modeling, and fabrication of microstructures, microsensors, and microactuators. He holds six U.S. patents in the area of MEMS.

Dr. Lin is the recipient of the 1998 NSF CAREER Award for research in MEMS packaging. He led the effort in establishing the MEMS subdivision in ASME and is currently serving as the Vice Chairman of the Executive Committee for the MEMS subdivision.

Huey-Chi Chu received the B.S. degree in mathematics and M.S. degree in applied mechanics from National Taiwan University, Taiwan, R.O.C., in 1994 and 1996, respectively.

Since 1996, he has been a process engineer for DRAM development at Vanguard International Semiconductor Corporation, Hsinchu, Taiwan, R.O.C.

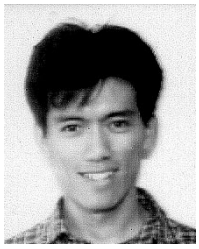

Yen-Wen Lu received the B.S. degree in agricultural machinery engineering from National Taiwan University, Taiwan in 1993 and the M.S. degree in mechanical engineering and applied mechanics from the University of Michigan in 1998. He is currently working toward the Ph.D. degree in the area of MEMS fabrication and CAD architecture at the University of California, Los Angeles.